ACS APPLIED MATERIALS & INTERFACES

Research Article

www.acsami.org

Target-Molecule-Triggered Rupture of Aptamer-Encapsulated Polyelectrolyte Microcapsules

Xueru Zhang,[†] Denise Chabot,[‡] Yasir Sultan,[‡] Carlos Monreal,[‡] and Maria C. DeRosa*[,†]

[†]Department of Chemistry, Carleton University, Ottawa, Canada

[‡]Agriculture and AgriFood Canada, Ottawa, Canada

Web-Enhanced Feature *Supporting Information*

ABSTRACT: Polyelectrolyte microcapsules have great potential for serving as carriers for the delivery of their contents when triggered by an external stimulus. Aptamers are synthetic ssDNA or RNA that can bind to specific targets with high affinity and selectivity. Aptamers may retain these superior molecular recognition properties after encapsulation within polymer microcapsules. In this work, stable polyelectrolyte microcapsules with encapsulated aptamers were obtained by the layer-by-layer (LbL) method. Polyelectrolyte films were deposited onto a $CaCO_3$ template that had been predoped with polystyrene sulfonate (PSS) and aptamer sequences (SA) that have an affinity for the dye sulforhodamine B (SRB). The PSS and aptamers are thought to serve as an internal scaffold supporting the microcapsule walls. These microcapsules would present target-molecule-triggered rupture properties. Microcapsule collapse was triggered by the binding of SRB to the encapsulated aptamer. The specificity of microcapsule collapse was investigated using a similar dye, tetramethylrosamine (TMR), which does not have affinity for SA. A high concentration of TMR did not lead to the collapse of the microcapsules. The effect of target binding on the microcapsules was confirmed by scanning electron microscopy (SEM) and confocal laser scanning microscopy (CLSM). These microcapsules may have potential applications in targeted delivery systems for the controlled release of drugs, pesticides, or other payloads.

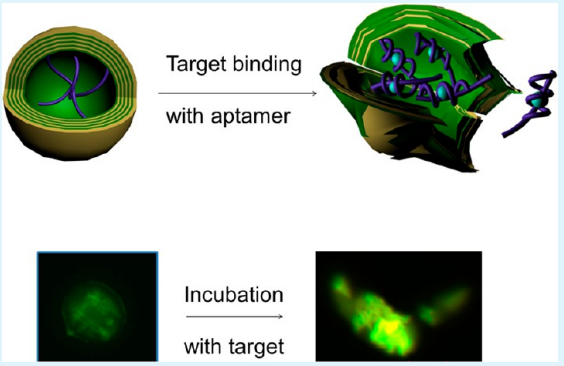

KEYWORDS: *aptamer, target molecule, triggered rupture, polyelectrolyte microcapsules, layer-by-layer assembly, selectivity*

1. INTRODUCTION

First introduced by Iler in 1966 and developed by the Decher group in the 1990s,[1] the layer-by-layer (LbL) assembly method has been widely used for preparing polyelectrolyte films, because of its simplicity and versatility, as well as its potential applications in sensing and controlled release systems.[2−4] Based on this approach, it is effective and convenient to assemble multilayered polyelectrolyte films on three-dimensional (3D) templates by exposing the charged substrates to oppositely charged polyelectrolyte solutions. Subsequent removal of the sacrificial templates under certain conditions can produce hollow capsules.[5,6] This powerful technique enables precise control of the thickness, structure, and composition of films on the nanoscale through the appropriate choice of deposition components, layer number, deposition order, or deposition conditions such as concentration, component charge density, temperature, pH, or ionic strength.[7−10] By utilizing the LbL method, external-stimuli-responsive polyelectrolyte microcapsules can be obtained.[11−13] These microcapsules can serve as targeted carriers to deliver their contents when triggered by external stimuli such as pH,[14] redox and electrical potential,[15] temperature,[16] ionic strength,[17] light,[18] or via enzymatic degradation,[19,20] which would change the wettability, adhesivity, permeability, porosity, or stability of the polyelectrolyte microcapsules and then lead to payload release. Among these stimuli-responsive systems, biodegradable polyelectrolyte microcapsules that can be used for drug delivery have attracted attention recently.[21−26] Biomaterials such as proteins can be trapped inside templates, using commonly used coprecipitation methods.[27,28] $CaCO_3$ and silica particles have been widely used as sacrificial templates for the preparation of hollow microcapsules.[29] Unlike silica, which requires harsh acidic conditions to dissolve the templates, $CaCO_3$ removal requires only a Ca^{2+} chelator (e.g., ethylenediaminetetraacetic acid, EDTA), making it an ideal template candidate when pH must be tightly controlled in order to maintain the activity and stability of the loaded biomaterials.[27]

Even though external-stimuli-responsive polyelectrolyte microcapsules have been extensively developed recently, there still remain challenges toward spatial and temporal controlled release of contents from microcapsules.[30] In the previously mentioned examples of responsive microcapsules, the release of contents is mainly triggered by external environments but not by the detection of a specific chemical signal. While there are examples of LbL microcapsules sensitive to chemical signals such as sugars[31] and biotin,[32] there are many other examples

Received: February 21, 2013
Accepted: May 24, 2013
Published: May 24, 2013

where target-molecule-triggered release of a payload could be extremely beneficial for precise spatial and temporal delivery.[33,34] Here, we propose a novel approach to construct "smart" systems by encapsulating aptamers within polyelectrolyte microcapsules. These microcapsules with added functionality could be used in many important areas, such as drug delivery or smart sensors. For example, an encapsulated drug could be released only upon detection of a specific chemical biomarker.

In the early 1990s, research groups led by Joyce,[35] Gold,[36] and Szostak[37] separately discovered that nucleic acid sequences can be evolved to bind to non-nucleic-acid targets with high affinity and selectivity. These antibody-like functional ssDNA and RNA molecules, generally composed of 15−60 nucleotides, were termed "aptamers". Aptamers can be generated by an in vitro screening process known as SELEX (Systematic Evolution of Ligands by Exponential Enrichment) starting from a random DNA/RNA pool.[38−42] SELEX allows for the discovery of aptamers for a variety of targets, ranging from small molecules (such as amino acids) to large protein complexes and even whole cells.[43−47] Upon binding with their target, aptamers will form a specific 3D conformation, which could include structural elements such as G-quadruplexes, hairpins, pseudoknots, or two- to five-way junctions.[48−50] The binding affinity of aptamers with their targets is typically assessed by using the dissociation constant (K_d).[51−55] A smaller K_d value designates a higher affinity. The reported K_d values for aptamers can be as low as within the nanomolar or even picomolar range.

Because of their robust molecular recognition properties, the use of aptamers as targeting ligands in drug delivery systems based on drug conjugates, micelles, liposomes, and polymer nanoparticle has received significant attention.[56−62] We have recently demonstrated that aptamers can serve as molecular recognition agents when embedded within multilayered polyelectrolyte film.[63] Furthermore, we have shown that when an aptamer housed within the wall of a polyelectrolyte microcapsule is exposed to its cognate target, that binding event can lead to an increase in the diffusion of that molecule through the microcapsule walls.[64] Thus, aptamers have the potential to serve as triggers for the controlled release of molecular payloads.

Our current goal is to further design a smart delivery system based on the high binding affinity and conformational flexibility of aptamers, where the release of a payload occurs concomitantly with detection and binding of target molecules. In this work, we prepared a model system for target-molecule-triggered microcapsule rupture. Prior to the addition of target molecules, free aptamers will serve as a part of an internal scaffold used to support the wall of a microcapsule.[65−68] After the addition of target molecules, the conformational change experienced by the aptamer during the formation of the aptamer−target complex could compromise the stability of that scaffold structure, leading to the collapse and rupture of the microcapsule, initiating payload release. A schematic picture for this process is shown in Figure 1. The introduction of a molecular recognition probe as a scaffold for the polyelectrolyte microcapsules could allow for controlled target-molecule-triggered release of contents under selective conditions.

In our work, we have tested this idea with the sulforhodamine B Aptamer (SA) as a model system.[64] SA was chosen because target binding can be easily monitored by confocal laser scanning microscopy (CLSM) measurements. In addition, a closely related dye, tetramethylrosamine (TMR), which is not recognized by SA, was used to test selectivity. By detecting whether microcapsules rupture in the presence of nontarget molecules such as TMR, one can verify the selectivity of this approach for triggered release.

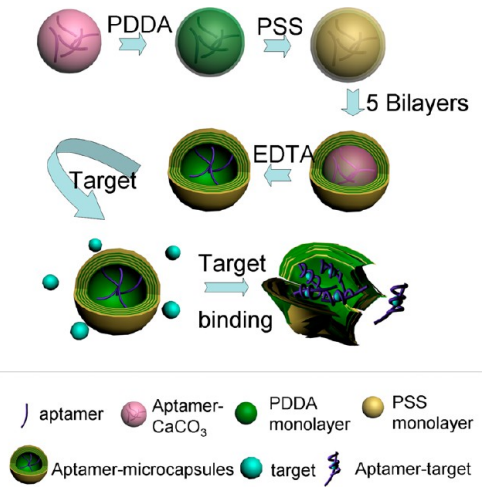

Figure 1. Experimental scheme depicting microcapsule preparation and target-induced microcapsule rupture. Target binding changes the conformation of the aptamers leading to the collapse of the microcapsule scaffold.

2. EXPERIMENTAL SECTION

2.1. Materials. Anhydrous calcium chloride (≥93.0%, granular), sodium bicarbonate (≥99.5%), PAH (polyallylamine hydrochloride) powder (average molecular weight of $M_w \approx 56\,000$), PDDA (polydiallyldimethylammonium chloride) 20% aqueous solution (average $M_w \approx 200\,000$), PSS powder (average $M_w \approx 70\,000$), and SRB powder were purchased from Sigma−Aldrich (Oakville, Ontario, Canada). EDTA was purchased from Bioshop (Burlington, Ontario, Canada). TMR powder was purchased from Invitrogen (Burlington, Ontario, Canada) and 5′-fluorescein phosphoramidite from Glen Research (Sterling, VA, USA). SA with a sequence of 5′-CCG GCC TAG GGT GGG AGG GAG GGG GCC GG-3′, with and without fluorescein tagging at the 5′ end, was synthesized on a MerMade 6 DNA synthesizer by standard phosphoramidite chemistry.

2.2. Fabrication of SA:PSS-$CaCO_3$ Particles. SA:PSS-$CaCO_3$ particles that could serve as templates for the polyelectrolyte microcapsules were prepared by a coprecipitation process in the presence of small amounts of PSS and SA. In these SA:PSS-$CaCO_3$ templates, SA and PSS would work together as a scaffold to support the microcapsules. Within a 1 mL reaction, PSS (0.13 mg) and SA (0.64 mg) were first dissolved in 0.33 M $NaHCO_3$ solution and then mixed with $CaCl_2$ solution (0.33M) under vigorous stirring (1000 rpm) at 10 °C for 20 s. After this, the solution was left unstirred for 6 min. The particles were then filtered and dried overnight.

2.3. Fabrication of SA:PSS-$(PDDA/PSS)_5$ Microcapsules. One milligram (1 mg) of the SA: PSS-$CaCO_3$ particles were incubated with 1 mL of a 3 mg/mL PDDA-0.5 M NaCl solution and 1 mL of a 3 mg/mL PSS-0.5 M NaCl solution, alternatively, for 30 min at a time and with intermittent centrifugation and washing steps to prepare $(PDDA/PSS)_5$-coated particles. Microcapsules were obtained by dissolving the $CaCO_3$ with 0.5 M EDTA, pH 6.97. This high concentration of EDTA was crucial to completely remove all of the $CaCO_3$. Excess EDTA was removed by washing with distilled water.

2.4. Triggered Rupture Properties of SA:PSS-$(PDDA/PSS)_5$ Microcapsules. The rupture of aptamer-encapsulated polyelectrolyte microcapsules triggered by aptamer−target binding would be a function of target concentration and incubation time. Before designing experiments to unravel the required parameters for the triggered rupture of the SA:PSS-$(PDDA/PSS)_5$ microcapsules, the molarity of aptamers in each microcapsule needed to be calculated. The loss of SA

dx.doi.org/10.1021/am400668q | ACS Appl. Mater. Interfaces 2013, 5, 5500−5507

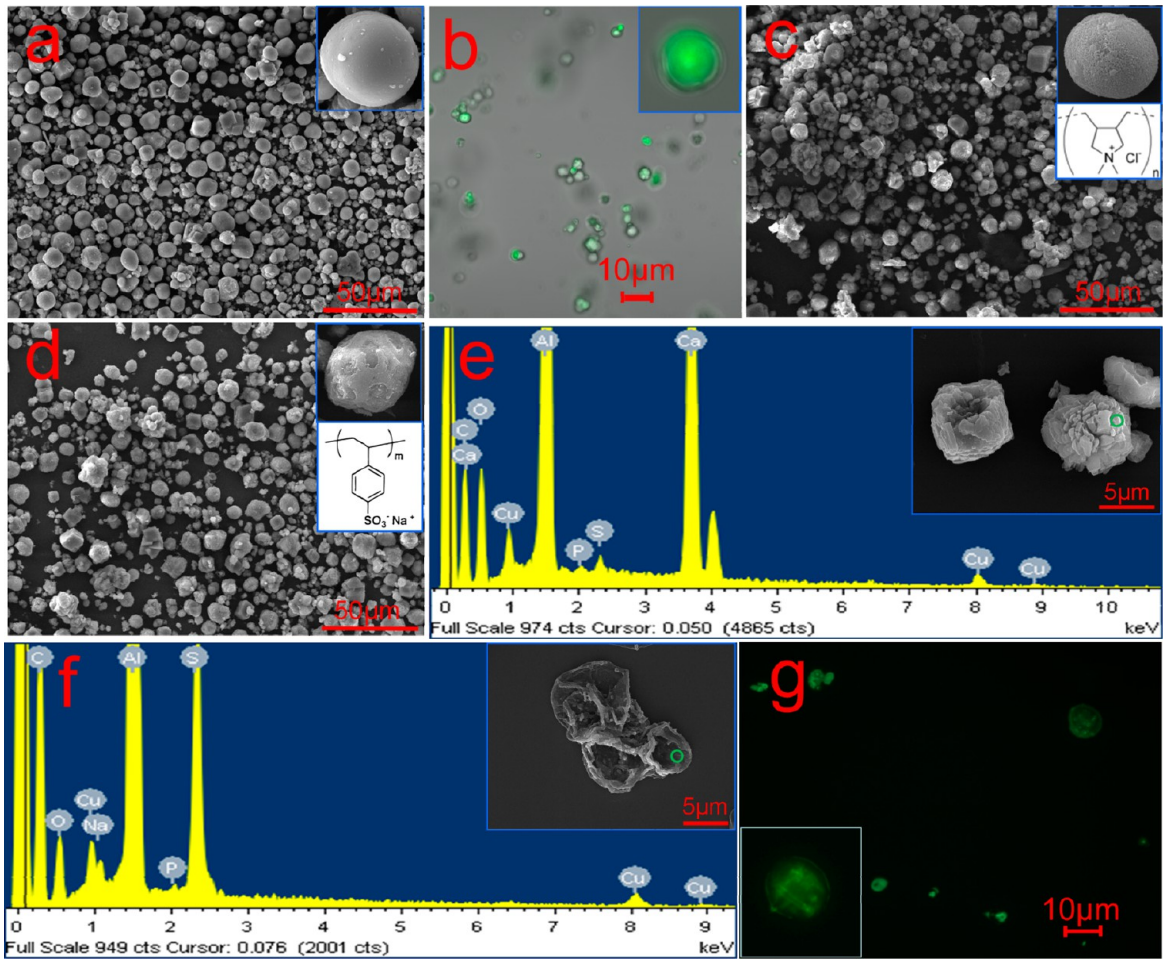

Figure 2. (a) SEM image of SA:PSS-$CaCO_3$ particles; inset shows an enlarged image of one particle. (b) CLSM image of SA:PSS-$CaCO_3$ particles prepared with fluorescein-labeled aptamers; inset shows an enlarged image of one particle. (c) SEM image after deposition of one layer of PDDA onto SA:PSS-$CaCO_3$ particles; the upper inset shows an enlarged image of one particle, and the lower inset shows the PDDA chemical structure. (d) SEM image after coating one bilayer of PDDA/PSS; the upper inset shows an enlarged image of one particle, and the lower inset shows the PSS chemical structure. (e) EDX spectrum of SA:PSS-$CaCO_3$ particles after coating with $(PDDA/PSS)_5$ films; inset shows its SEM image. (Signals from Ca, C, S, and P confirm the presence of the aptamer and PSS within the coated templates.) (f) EDX spectrum of dried SA:PSS-$(PDDA/PSS)_5$ microcapsules (after $CaCO_3$ dissolution); inset shows its SEM image. (All selected areas for EDX measurements were marked by the green ring. Once again, the presence of P confirms the aptamer loading within the microcapsules. N.B. Al studs contain Al with trace impurities, such as C, O, Cu, or Na.) (g) CLSM image of SA:PSS-$(PDDA/PSS)_5$ microcapsules prepared from fluorescein-labeled aptamers; inset shows an enlarged image of one capsule.

during deposition and dissolution steps was estimated by monitoring the fluorescein signal in the emission spectrum of the supernatant solution (see Figure S3 in the Supporting Information). The maximum aptamer concentration (after accounting for this loss) in each microcapsule was estimated to be 2.3 mM (see the Supporting Information).

The dissociation constant (K_d) for SA and SRB can be calculated using the following equation:[70−73]

$$K_d = \frac{[A][T]}{[C]}$$

where [A] refers to the free aptamer concentration, [T] is the free target molecule concentration, and [C] is the aptamer−target complex concentration at the equilibrium point. The K_d values for SA and SRB have been reported to be 660 ± 60 nM.[69] Therefore, two SRB concentrations were chosen to check the triggered rupture properties of the microcapsules:

(1) *Low target concentration.* When the SRB concentration is 10 μM, [dye] × [Aptamer] = 23 nM < K_d, which means that only a low proportion of aptamers will be bound in a complex.

(2) *High target concentration.* When SRB concentration is increased to 1 mM, [dye] × [Aptamer] = 2.3 μM > K_d, then almost all aptamers will be bound in a complex.

The obtained microcapsules were incubated with 50 μL of the SRB solutions in 0.1 M KCl for 16 h, 1 day, and 6 days, respectively. In these samples, 1 μL solution is estimated to contain ∼200−220 microcapsules. (See the Supporting Information.) After incubation, all samples were centrifuged and washed three times with distilled water to remove any extra dye. The status of the SA:PSS-$(PDDA/PSS)_5$ microcapsules then was tested to unravel the parameters for triggered rupture. The shape and surface morphology of these microcapsules after incubation under each condition was monitored by backscattered electron images (BEIs) from scanning electron microscopy (SEM), and the rupture/collapse of the microcapsules was determined by examining their change of shape and surface morphology. At least three images of each sample obtained from different areas were manually counted in order to calculate the percentage of ruptured/collapsed microcapsules; normally in each image, more than 100 microcapsules were examined to calculate the average percentages of ruptured, collapsed, or intact microcapsules in each sample.

dx.doi.org/10.1021/am400668q | ACS Appl. Mater. Interfaces 2013, 5, 5500−5507

2.5. Selectivity of SA:PSS-(PDDA/PSS)$_5$ Microcapsules. SA:PSS-(PDDA/PSS)$_5$ microcapsules were also incubated in a nontarget molecule (TMR) solution under the same dye concentration and incubation times as SRB, in order to check the selectivity of microcapsules. The morphological changes were examined by SEM and CLSM.

2.6. Measurements. Tescan VegaII XMU SEM with a secondary electron (SE) detector was used to check sample morphologies under dry conditions. These dried samples were uniformly spread on aluminum studs and then sputtered with a thin layer of gold film. Tescan VegaII XMU Cryo stage SEM with a backscattered electron (BSE) detector in a low vacuum environment under a nitrogen pressure of 10 Pa at −30 °C was used to examine hydrated samples. The hydrated samples were prefrozen at −80 °C to preserve their morphologies. The elemental analysis (energy-dispersive X-ray analysis) was conducted using an Oxford EDS instrument with an INCAx-act Detector. INCA Energy software was used for analysis.

The samples for CLSM measurements were first dispersed into 10 μL of deionized (DI) water, and then put onto glass slides. After drying overnight, samples were mounted in Fluoromount G from EMS (Hatfield, PA) and covered with a high-performance coverslip of 0.17 mm thickness from Zeiss (Toronto, Ontario, Canada). Images were acquired on Confocal Zeiss LSM510 META with a Plan-Apochromat 63×/1.4 Oil DIC objective and electronic zoom 5. Fluorescence was observed using the Argon/2 laser 488 nm excitation line with emission BP (Band Pass) 505−550 nm for fluorescein and exciting laser DPSS 561 with emission LP (Long Pass) 575 nm for SRB and TMR. Z-stack images of samples were obtained by taking many slice images at ∼0.8 μm intervals along the *Z*-axis.

3. RESULTS AND DISCUSSION

3.1. SA:PSS-(PDDA/PSS)$_5$ Microcapsules. Biomaterials, such as aptamers, can be loaded into the core of spherical $CaCO_3$ particles that serve as sacrificial templates for polyelectrolyte microcapsules. Optimization studies with the goal of increasing the yield of spherical $CaCO_3$ particles were performed and monitored using SEM (see the Supporting Information). Collectively, a salts concentration of 0.33 M, a temperature of 10 °C, and an incubation time of 6 min were found to be the best conditions for fabricating spherical $CaCO_3$ particles (see Figure S1a in the Supporting Information). The size of the obtained spherical $CaCO_3$ particles was in the range of 4−6 μm, in agreement with what has been observed in the literature.[28] Different amounts of fluorescein-tagged SA aptamers (Fluorescein-SA) then were loaded into the $CaCO_3$ via a coprecipitation process, using a range of SA:$CaCO_3$ feed mass ratios to obtain the optimal SA loading. The success of loading was confirmed by CLSM. The CLSM images indicated that, when the reaction mass ratio between SA and $CaCO_3$ was 1:47, green fluorescence from the fluorescein-SA was mostly visible inside the $CaCO_3$. (See Figure S1b in the Supporting Information.) With the loaded aptamer, the particles were still in 4−6 μm range and remained spherical (see Figure S1c in the Supporting Information). The particle surfaces were as smooth as those without embedded aptamers. Thus, aptamer encapsulation did not change the overall particle morphology. The template was further modified by introducing a small amount of PSS into the $CaCO_3$, along with SA during the coprecipitation process.[74] In previous studies, loaded PSS was shown to be released from $CaCO_3$ during the dissolution process and to bond instantaneously with the oppositely charged polyelectrolytes that have been deposited on $CaCO_3$, increasing the stability of the microcapsules.[75,76] An SEM image of these templates is shown in Figure 2a. Approximately 0.4% feed mass ratio PSS was introduced to prepare the SA:PSS-$CaCO_3$ particles and the result was that particles were mostly spherical with smooth surfaces. In addition, batches of SA:PSS-$CaCO_3$ particles contained a higher percentage of spherical particles overall, compared with that obtained for SA-$CaCO_3$ particles under the same reaction conditions. After doping with PSS, aptamer loading in the SA:PSS-$CaCO_3$ was confirmed by CLSM. (See Figure 2b.) Z-stack images of SA:PSS-$CaCO_3$ particles clearly show the three-dimensional (3D) distribution of the aptamers within the particles. (See Supplemental Video 1.)

Polyelectrolyte combinations were then deposited onto our templates by the LbL process to fabricate microcapsules. In our initial studies, PAH/PSS pairs were used (see the Supporting Information). Unfortunately, the obtained microcapsules were mostly agglomerates, and when the number of film deposition steps was reduced in order to decrease the possibility of agglomeration, most of the microcapsules broke upon template dissolution. Thus, PDDA was used as the polycation as a replacement for PAH. PDDA is a pH-insensitive quaternary ammonium polycation and has high charge density over all pH ranges.[77] The particle morphologies after coating one layer of PDDA were checked by SEM. The results showed that the particles remained spherical with their surfaces completely covered with a condensed film (see Figure 2c). When the deposition process was continued to add a PSS layer, the roughness became obvious on the surface of most particles (see Figure 2d). The formation of this rough structure may be caused by the interpenetration of PDDA and PSS, as they diffuse "in" or "out" of film grooves and grow in exponential mode.[78] After deposition of the (PDDA/PSS)$_5$ film onto the SA:PSS-$CaCO_3$ particles, there was no indication of agglomeration that had plagued the PAH/PSS-coated particles and the particles displayed a flower-like surface structure (see Figure 2e). EDX analysis confirmed that the (PDDA/PSS)$_5$-coated SA:PSS-$CaCO_3$ particles contain Ca (from $CaCO_3$), S (from PSS), and P (from the aptamer) (see Figure 2e). This indicated that some aptamers remained inside the particles during film coating. After dissolution of the $CaCO_3$, the SA:PSS-(PDDA/PSS)$_5$ microcapsules imaged under dry conditions appeared flat on the substrate (see Figure 2f). The size of the individual microcapsules was within the expected range of 4−6 μm, which proved that no aggregation occurred during the PDDA/PSS film deposition or dissolution process. EDX (Figure 2f) showed that Ca was no longer present within microcapsules, which confirmed the thorough dissolution of $CaCO_3$ by supersaturated EDTA solution. The main component in this sample was C, from the backbone of PDDA, PSS, and aptamers. Similarly, S and P could still be detected, confirming the presence of PSS and aptamers. As a result, aptamer-loaded (PDDA/PSS)$_5$ microcapsules were successfully fabricated. SA loss during film deposition and template dissolution steps was monitored by fluorescence (see Figure S3 in the Supporting Information). The data suggest that, during the microcapsule fabrication process, ∼30% of SA is lost. The greatest loss occurs during the initial film deposition steps, perhaps because of the displacement of loosely held aptamers at or near the surface of the templates. After dissolution of the $CaCO_3$, the remaining aptamer would be released from the templates and bond with the (PDDA/PSS)$_5$ films. Some SA loss at this stage suggests that the microcapsule walls are somewhat permeable to the aptamers. Indeed, polyelectrolyte multilayer capsules have been shown to be somewhat permeable to DNA.[79] CLSM images were used to confirm the presence and check the distribution of aptamer within the SA:PSS-(PDDA/PSS)$_5$ microcapsules (see

Figure 2g). These images clearly indicated that aptamers had two different distributions within the microcapsules. Some images show the aptamer as a green ring in the microcapsule wall; or, if microcapsules contain more aptamer, it was distributed throughout the microcapsules as a green diffuse circle. The 3D distribution of aptamers within an individual microcapsule was checked by Z-stack images. (See Supplemental Video 2.) These Z-stack images verify the intact structure of the microcapsules and the encapsulation of SA.

3.2. Triggered Rupture Properties of SA:PSS-(PDDA/PSS)$_5$ Microcapsules. If these microcapsules are incubated in water, intact ones will absorb water and become swollen spherical structures,[80] while any broken microcapsules will be observed as a ruptured structure. Cryo-stage SEM measurements preserve the absorbed water within the microcapsules and allow for differentiation between complete and broken ones. Therefore, after incubation of microcapsules in target- or nontarget-molecule solution, their status was visualized using cryo-stage SEM under frozen conditions. (PDDA/PSS)$_5$-coated SA:PSS-$CaCO_3$ particles and SA:PSS-(PDDA/PSS)$_5$ microcapsules were first imaged as controls. Under frozen conditions, (PDDA/PSS)$_5$-coated SA:PSS-$CaCO_3$ particles (Figure 3a) do not show any structural differences, as compared with dry conditions. All particles still looked like "flowers" without any rearrangements and aggregation. Because cryo-stage SEM images were obtained in a low-vacuum nitrogen environment, they were not as clear as the gold coated images. Under frozen conditions, the SA:PSS-(PDDA/PSS)$_5$ microcapsules after template dissolution appeared as transparent, semiswollen structures, because of the absorbed water present inside the microcapsule wall (see Figure 3b).

We then sought to test the effect of target binding on microcapsule morphology. The initial thought was that microcapsules may burst after incubation in a 1 mM SRB−0.1 M KCl solution for several hours. The SA aptamer dissociation constant is in the range of 700 nM; therefore, in the presence of a high concentration of the SRB (1 mM), a large proportion SA should bind with SRB and form a SA-SRB complex. The binding and folding of the aptamer may compromise its ability to support the stability of microcapsules, allowing for the collapse/rupture of the microcapsules. SRB was dissolved in 0.1 M KCl solutions for the incubation experiments as K^+ stabilizes SA in a G quartet structure and is required for target binding.[69]

The cryo-stage SEM images have shown that, after the microcapsules were incubated in 1 mM SRB−0.1 M KCl for 16 h (Figure 3c), most microcapsules were intact and appeared as swollen, spherical structures with only ∼2% found to be collapsed, as determined by manual counting of capsules in the image (see the Experimental Section). Thus, it was reasoned that more time may be required to bind to the target molecules, form G quartet structures, and drive the collapse of the microcapsules. When the incubation time was prolonged to 1 day (24 h) in 1 mM SRB−0.1 M KCl, almost all microcapsules were collapsed with ∼1% remaining in a spherical shape (see Figure 3d). When incubated in 1 mM SRB−0.1 M KCl for 6 days, 60% of the microcapsules appeared not only to be flattened but also to have burst (see Figure 3e). In the burst microcapsules, only the bottom wall can be observed.

Microcapsules were also incubated with low concentrations of target (10 μM SRB−0.1 M KCl solution) for 1 day (24 h) and 6 days to ensure that the collapse and rupture of the microcapsules were caused by the formation of SA-SRB

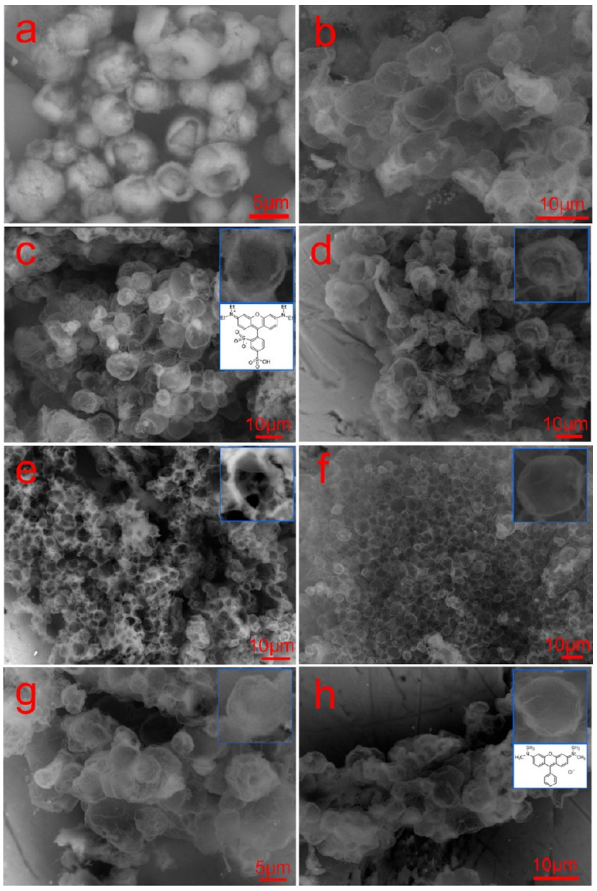

Figure 3. Cryo-stage SEM images of (a) (PDDA/PSS)$_5$-coated SA:PSS-$CaCO_3$ particles, (b) frozen SA:PSS-(PDDA/PSS)$_5$ microcapsules, (c−e) SA:PSS-(PDDA/PSS)$_5$ microcapsules after incubation in 1 mM SRB−0.1 M KCl solution for different times ((c) 16 h, (d) 1 day, and (e) 6 days). The chemical structure of SRB is shown in panel (c). Cryo-stage SEM images of SA:PSS-(PDDA/PSS)$_5$ microcapsules after incubation in 10 μM SRB−0.1 M KCl at (f) 1 day and (g) 6 days. (h) SA:PSS-(PDDA/PSS)$_5$ microcapsules after incubation in 1 mM TMR−0.1 M KCl for 6 days; the lower inset shows the chemical structure of TMR. All insets of SEM images are enlarged images of single microcapsules obtained from the corresponding SEM image.

complexes within the microcapsule. As calculated in the Experimental Section, in 10 μM SRB, a very low proportion of aptamers will be bound as aptamer−target complexes, so most aptamers can still serve as a scaffold to support the stability of microcapsules. Under low concentration conditions after 1 day, >99% of the microcapsules remained as swollen spherical structures (see Figure 3f). Comparing these microcapsules with those that had been incubated in 1 mM SRB for 1 day, this result suggested that the collapse of microcapsules at high target molecule concentration was not simply due to the long incubation time. When microcapsules were incubated in 10 μM SRB-0.1 M KCl for 6 days, the great majority of them remained as intact spherical structures (see Figure 3g). Again, this confirmed that the long incubation time alone was not the cause of capsule rupture.

To further confirm that the effect on microcapsule morphology was driven by aptamer−target binding, samples were checked by CLSM colocalization experiments. These colocalization images were obtained by exciting the samples with two different laser sources and then checking the presence and location of two different dyes simultaneously. As in

dx.doi.org/10.1021/am400668q | ACS Appl. Mater. Interfaces 2013, 5, 5500−5507

previous studies, the green color in these images comes from fluorescein-labeled aptamers, while the orange color denotes SRB emission and any yellow color will indicate the colocalization of fluorescein aptamers and SRB. Microcapsules incubated for 6 days under different conditions were examined via CLSM measurements. After incubation in 10 μM SRB−0.1 M KCl for 6 days, as shown in Figure 4a, the majority of the

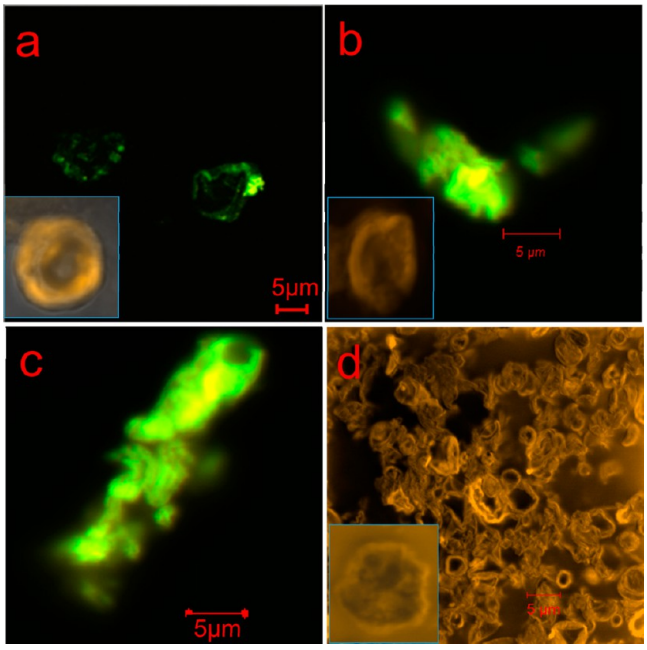

Figure 4. (a−c) Colocalization experiments to confirm SA−SRB binding and triggered rupture properties of microcapsules. The images were taken after incubation at different SRB concentrations for 6 days (a) in 10 μM SRB−0.1 M KCl and (b, c) in 1 mM SRB−0.1 M KCl (same sample from different areas). All insets show orange channel emission image from nonfluorescein aptamer microcapsules. (d) CLSM images for selectivity study of microcapsules after incubation in 1 mM TMR−0.1 M KCl for 6 days, obtained from orange channel emission; inset shows an enlarged image of one microcapsule.

fluorescent signal was coming from fluorescein aptamers, present on the walls of the microcapsules. The aptamer and SRB signals were not completely overlaid, and only very little yellow color can be observed. In this sample, the low amount of SRB available to the microcapsules allows few SA−SRB complexes to be formed. Z-stack images obtained from the green channel of this sample demonstrate that the aptamer signal has a similar 3D contour as the individual microcapsules which confirm that the microcapsule is intact. (See Supplemental Video 3.) CLSM measurements were also conducted using unlabeled (no fluorescein) aptamer-encapsulated microcapsules after incubation under the same conditions (see inset in Figure 4a). The images indicated that SRB can permeate into the microcapsules and remain there, because the orange color could be visualized wrapped by the colorless microcapsule wall. These CLSM images confirm that, when only a low number of SA−SRB complexes formed, most of the aptamers can still work as a scaffold and keep the microcapsules complete.

In contrast, in CLSM images for microcapsules incubated in 1 mM SRB−0.1 M KCl for 6 days, polymer debris can be observed throughout the image (see Figures 4b and 4c). In this debris, the intensity of the SRB signals is significantly increased and the fluorescein aptamer signal still remains, so almost all the debris presented a yellow color. This bright yellow color suggests that most aptamers are colocalized with SRB and formed complexes. The conformational change of the aptamer may have led to the collapse and rupture of the microcapsules, leaving only the polymer debris. No Z-stack images could be obtained because of their lack of structure. Once again, unlabeled aptamer-encapsulated microcapsules were also incubated in 1 mM SRB for 6 days and measured by CLSM. In this image, in addition to the polymer debris, broken microcapsules with SRB's orange color could still be detected (see inset in Figure 4b). This image suggests that the rupture of microcapsules was caused by SA−SRB binding at SRB concentrations higher than the dissociation constant of the aptamer. In addition, we attempted to measure the degree of SA release after 6 days in SRB−0.1 M KCl solution by UV−vis spectroscopy. Unfortunately, any DNA absorbance was masked by the large background signal from SRB (results not shown). From the confocal images, however, it is clear that a large fluorescein signal from SA is present with the polymer debris, which suggests that most of the aptamer remains in close proximity to the polyelectrolyte layers, perhaps by electrostatic interactions.

Overall, these results suggest that SRB had permeated into the SA encapsulated microcapsules over the 6 days of incubation. When the SRB concentration was increased and more SA−SRB complexes were formed, microcapsule collapse and rupture were observed.

3.3. Selectivity of SA:PSS-(PDDA/PSS)$_5$ Microcapsules.

To confirm that the high concentration of any dye will not lead to microcapsule rupture simply because of osmotic pressure, the experiments were repeated with TMR as the target. TMR has a similar chemical structure to SRB, which is composed of a three-ring xanthene. However, because of the discriminatory nature of aptamers, SA does not bind with high affinity to TMR. Incubation of the microcapsules in TMR served as a control to check the selectivity of this observed morphology change. After incubation in 1 mM TMR−0.1 M KCl for 6 days, 85% of the microcapsules appeared intact by SEM and remained as spherical structures, with the others looking somewhat collapsed (see Figure 3h). This result revealed that the rupture of microcapsules in 1 mM SRB was not caused simply by a high osmotic pressure of dye molecules. Furthermore, microcapsules encapsulated with fluorescein aptamers were incubated in 1 mM TMR−0.1 M KCl for 6 days and run on the CLSM. The image obtained from the orange channel showed that TMR remained mostly outside of the microcapsules, because the intensity of the orange color was strongest in the microcapsule wall and also in the background (see Figure 4d). The microcapsules appear to be intact or slightly collapsed but not ruptured at a high concentration of nontarget molecule solution. Comparing results obtained from incubations with 1 mM SRB−0.1 M KCl, aptamer-loaded microcapsules exhibited high selectivity and microcapsule rupture was only noted after the binding of the aptamer with target molecules and the formation of aptamer−target complexes. This could have exciting implications in the area of controlled release as the triggered rupture of these microcapsules could be tailored to allow for the release of their contents, in response to the detection of specific target molecules.

dx.doi.org/10.1021/am400668q | ACS Appl. Mater. Interfaces 2013, 5, 5500−5507

4. CONCLUSION

The layer-by-layer (LbL) assembly process on SA:PSS-loaded $CaCO_3$ templates was a suitable method for the preparation of stable aptamer-encapsulated microcapsules. SA:PSS-$(PDDA/PSS)_5$ microcapsules demonstrated target-molecule-triggered morphology changes. The rupture of these microcapsules seems to be controlled by target-molecule concentration and incubation time. We have previously demonstrated that the target-binding-induced conformational change of aptamers that were embedded within the microcapsule walls can lead to increased permeability.[64] In this study, the aptamer-encapsulated microcapsules went through apparent collapse and rupture, potentially due to the conformational change of the aptamer that was serving as a structural support. The relationship between microcapsule morphology, target-molecule concentration, and incubation time is summarized in Figure 5. Under low-target-molecule-concentration conditions,

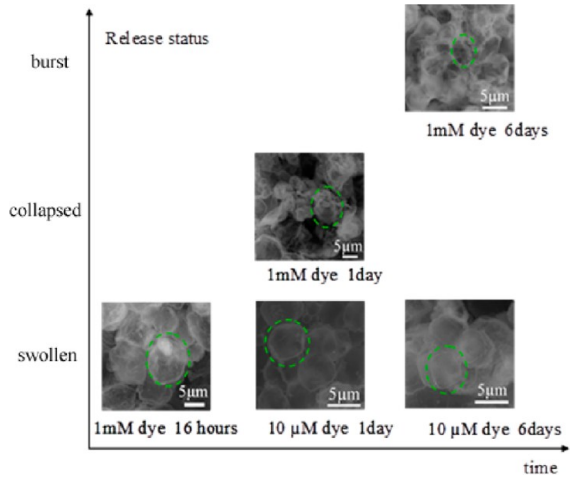

Figure 5. Microcapsule status as a function of incubated dye concentration and time; a swollen, collapsed, or burst microcapsule is highlighted by the green rings.

the microcapsules seemed to be stable and displayed complete spherical structures over several days of incubation. On the other hand, under high-target-molecule-concentration conditions, microcapsules went through swollen, collapsed, and ruptured states.

Aptamer-encapsulated microcapsules only burst in response to target molecules, while in nontarget-molecule solution, they remained as intact structures. So microcapsules encapsulated with aptamers exhibit additional functionality over conventional microcapsules. The release of contents from microcapsules concomitant with the detection of target molecules would be beneficial for targeted delivery. In the future, these functionalized microcapsules may be used in a "smart" delivery system. Ideally, the release of a payload such as a drug could be synchronized with the detection of a molecular signal, e.g. a biomarker that is spatially and temporally associated with a diseased tissue. Toward this goal, the effect of temperature, ionic strength, or pH on the stability of SA:PSS-$(PDDA/PSS)_5$ microcapsules will need to be examined. Stability *in vivo* will also need to be explored. Our preliminary stability experiments in sheep serum (see Figure S4 in the Supporting Information) are promising and will be further examined in future work.

■ ASSOCIATED CONTENT

Ⓢ Supporting Information

This Supporting Information contains experimental details as well as discussion on the synthesis of $CaCO_3$ particles, SA-$CaCO_3$ particles, SA-$(PAH/PSS)_x$ microcapsules, SA:PSS-(PAH/PSS) microcapsules, parametric validations for multilayer film formations, release percentage of SA during microcapsules fabrication, and a small trial for stability of microcapsules in serum. This material is available free of charge via the Internet at http://pubs.acs.org.

Ⓦ Web-Enhanced Features

Videos showing the Z-stack images and 3D distribution of aptamers within SA:PSS-CaCO3 particles and individual SA:PSS-(PDDA/PSS)5 microcapsules before and after incubation with SRB.

■ AUTHOR INFORMATION

Corresponding Author

*E-mail: maria_derosa@carleton.ca.

Notes

The authors declare no competing financial interest.

■ ACKNOWLEDGMENTS

The research was financially supported by NSERC, Agrium Advanced and Agriculture and Agri-Food Canada. We thank Dr. Farid Bensebaa at the National Research Council Canada for his kind support in using Zetasizer equipment. We thank Dr. Jianqun Wang for his support with the SEM and EDS measurements and determination. We thank Dr. Barbara Blackwell at Agriculture and Agri-Food Canada for access to confocal microscope facilities.

■ REFERENCES

(1) Iler, R. K. *J. Colloid Interface Sci.* **1966**, *21*, 569−594.
(2) Decher, G. *Science* **1997**, *277*, 1232−1237.
(3) Decher, G.; Hong, J. D.; Schmitt, J. *Thin Solid Films* **1992**, *210*, 831−835.
(4) Tang, Z.; Wang, Y.; Podsiadlo, P.; Kotov, N. A. *Adv. Mater.* **2006**, *18*, 3203−3224.
(5) Palama, I. E.; Coluccia, A. M. L.; Torre, A. D.; Vergaro, V.; Perrone, E.; Cingolani, R.; Rinaldi, R.; Leporatti, S. *Sci. Adv. Mater.* **2010**, *2*, 138−150.
(6) Voigt, A.; Lichtenfeld, H.; Sukhorukov, G. B.; Zastrow, H.; Donath, E.; Baumler, H.; Mohwald, H. *Ind. Eng. Chem. Res.* **1999**, *38*, 4037−4043.
(7) Decher, G.; Eckle, M.; Schmitt, J.; Struth, B. *Curr. Opin. Colloid Interface Sci.* **1998**, *3*, 32−39.
(8) Anzai, J.; Kobayashi, Y.; Nakamura, N.; Nishimura, M.; Hoshi, T. *Langmuir* **1999**, *15*, 221−226.
(9) Serizawa, T.; Yamaguchi, M.; Akashi, M. *Macromolecules* **2002**, *35*, 8656−8658.
(10) Caruso, F.; Niikura, K.; Furlong, D. N.; Okahata, Y. *Langmuir* **1997**, *13*, 3427−3433.
(11) Sukhishvili, S. A. *Curr. Opin. Colloid Interface Sci.* **2005**, *10*, 37−44.
(12) Anandhakumar, S.; Nagaraja, V.; Ashok, M. R. *Colloid Surf. B* **2010**, *78*, 266−274.
(13) Wohl, B. M.; Engbersen, J. F. J. *J. Controlled Release* **2012**, *158*, 2−14.
(14) Takayuki, I.; Toshiyuki, K.; Michiya, M.; Mitsuru, A. *Macromolecules* **2010**, *10*, 271−277.
(15) Haynie, D. T.; Palath, Y.; Liu, Y.; Li, B. Y.; Pargonkar, N. *Langmuir* **2005**, *21*, 1136−1138.
(16) Wang, F.; Zhu, Y.; Gao, C. *Colloid Surf. A* **2009**, *349*, 55−60.

(17) Mercato, L. L.; Abbasi, A. Z.; Parak, W. J. *Small* **2011**, *7*, 351−363.
(18) Bedard, M. F.; Geest, B. G.; Skirtach, A. G.; Moehwald, H.; Sukhorukov, G. B. *Adv. Colloid Interface Sci.* **2010**, *158*, 2−14.
(19) Johnston, A. P. R.; Lee, L.; Wang, Y.; Caruso, F. *Small* **2009**, *5*, 1418−1421.
(20) Ochs, C. J.; Such, G. K.; Caruso, F. *Langmuir* **2011**, *27*, 1275−1280.
(21) Johnston, A. P. R.; Kamphuis, M. M. J.; Such, G. K.; Scott, A. M.; Nice, E. C.; Heath, J. K.; Caruso, F. *ACS Nano* **2012**, *6*, 6667−6674.
(22) Cui, J.; Yan, Y.; Such, G. K.; Liang, K.; Ochs, C. J.; Postma, A.; Caruso, F. *Biomacromolecules* **2012**, *13*, 2225−2228.
(23) Becker, A. L.; Johnston, A. P. R.; Caruso, F. *Small* **2010**, *6*, 1836−1852.
(24) Borodina, T.; Markvicheva, E.; Kunizhev, S.; Mohwald, H.; Sukhorukov, G. B.; Kreft, O. *Macromol. Rapid Commun.* **2007**, *28*, 1894−1899.
(25) Geest, B. G.; Sanders, N. N.; Sukhorukov, G. B.; Demeester, J.; Smedt, S. C. *Chem. Soc. Rev.* **2006**, *36*, 636−649.
(26) Vergaro, V.; Scarlino, F.; Bellomo, C.; Rinaldi, R.; Vergara, D.; Maffia, M.; Baldassarre, F.; Giannelli, G.; Zhang, X.; Lvov, Y. M.; Leporatti, S. *Adv. Drug Delivery Rev.* **2011**, *63*, 847−864.
(27) Petrov, A. I.; Volodkin, D. V.; Sukhorukov, G. B. *Biotechnol. Prog.* **2005**, *21*, 918−925.
(28) Volodkin, D. V.; Larionova, N. I.; Sukhorukov, G. B. *Biomacromolecules* **2004**, *5*, 1962−1972.
(29) Jiang, X. M.; Chen, Z. C.; Lv, D. S.; Wu, Q.; Lin, X. F. *Macromol. Chem. Phys.* **2008**, *209*, 175−183.
(30) Muro, S. *J. Controlled Release* **2012**, *164*, 125−137.
(31) Sato, K.; Imoto, Y.; Sugama, J.; Seki, S.; Inoue, H.; Odagiri, T.; Hoshi, T.; Anzai, J. I. *Langmuir* **2005**, *21*, 797−799.
(32) Inoue, H.; Sato, K.; Anzai, J. I. *Biomacromolecules* **2005**, *6*, 27−29.
(33) Kemmer, C.; Fluri, D. A.; Witschi, U.; Passeraub, A.; Gutzwiller, A.; Fussenegger, M. *J. Controlled Release* **2011**, *150*, 23−29.
(34) Chan, T.; Gu, F. *Expert Rev. Mol. Diagn.* **2011**, *11*, 487−496.
(35) Robertson, D.; Joyce, G. *Nature* **1990**, *344*, 467−468.
(36) Tuerk, C.; Gold, L. *Science* **1990**, *249*, 505−510.
(37) Ellington, A.; Szostak, J. *Nature* **1990**, *346*, 818−822.
(38) Wilson, C.; Szostak, J. W. *Nature* **1995**, *374*, 777−782.
(39) Mendonsa, S. D.; Bowser, M. T. *Anal. Chem.* **2004**, *76*, 5387−5392.
(40) Stoltenburg, R.; Reinemann, C.; Strehlitz, B. *Anal. Bioanal. Chem.* **2005**, *383*, 83−91.
(41) Yang, X. B.; Li, X.; Prow, T. W.; Reece, L. M.; Bassett, S. E.; Luxon, B. A.; Herzog, N. K.; Aronson, J.; Shope, R. E.; Leary, J. F.; Gorenstein, D. G. *Nucleic Acids Res.* **2003**, *31*, e54.
(42) Stoltenburg, R.; Reinemann, C.; Strehlitz, B. *Biomol. Eng.* **2007**, *24*, 381−403.
(43) Hermann, T.; Patel, D. J. *Science* **2000**, *287*, 820−825.
(44) Mann, D.; Reinemann, C.; Stoltenburg, R.; Strehlitz, B. *Biochem. Biophys. Res. Commun.* **2005**, *338*, 1928−1934.
(45) Blank, M.; Weinschenk, T.; Priemer, M.; Schluesener, H. *J. Biol. Chem.* **2001**, *276*, 16464−16468.
(46) Daniels, D. A.; Chen, H.; Hicke, B. J.; Swiderek, K. M.; Gold, L. A. *Proc. Natl. Acad. Sci. U.S.A.* **2003**, *100*, 15416−15421.
(47) McKeague, M.; DeRosa, M. C. *J. Nucleic Acids* **2012**, *2012*, 748913.
(48) Jones, L. A.; Clancy, L. E.; Rawlinson, W. D.; White, P. A. *Antimicrob. Agents Chemother.* **2006**, *50*, 3019−3022.
(49) Win, M. N.; Klein, J. S.; Smolke, C. D. *Nucleic Acids Res.* **2006**, *34*, 5670−5682.
(50) Ulrich, H.; Ippolito, J. E.; Pagan, R.; Eterovic, V. A.; Hann, R. M.; Shi, H.; Lis, J. T.; Eldefrawi, M. E.; Hess, G. P. *Proc. Natl. Acad. Sci. U.S.A.* **1998**, *95*, 14051−14056.
(51) Cao, X. X.; Li, S. H.; Chen, L. C.; Ding, H. M.; Xu, H.; Huang, Y. P.; Li, J.; Liu, N. L.; Cao, W. H.; Zhu, Y. J. *Nucleic Acids Res.* **2009**, *37*, 4621−4628.
(52) Tang, Z. W.; Guan, D. S.; Wang, K. M.; Shi, H.; Sefah, K.; Mallikratchy, P.; Chen, H. W.; Li, Y.; Tan, W. H. *Anal. Chem.* **2007**, *79*, 4900−4097.
(53) Kleinjung, F.; Klussmann, S.; Erdmann, V. A.; Scheller, F. W.; Furste, J. P.; Bier, F. F. *Anal. Chem.* **1998**, *70*, 328−331.
(54) Buff, M. C. R.; Schafer, F.; Wulffen, B.; Muller, J.; Potzsch, B.; Heckel, A.; Mayer, G. *Nucleic Acids Res.* **2010**, *6*, 2111−2117.
(55) Guan, D. S.; Li, Y.; Tang, Z.; Cao, Z.; Chen, H.; Mallikaratchy, P.; Sefah, K.; Yang, C.; Tan, W. *Proc. Natl. Acad. Sci. U.S.A.* **2006**, *103*, 11838−11843.
(56) Ray, P.; White, R. R. *Pharmaceuticals* **2010**, *3*, 1761−1778.
(57) Ray, P.; Cheek, M. A.; Sharaf, M. L.; Li, N.; Ellington, A. D.; Sullenger, B. A.; Shaw, B. R.; White, R. R. *Nucleic Acid Ther.* **2012**, *22*, 295−305.
(58) Kang, H.; O'Donoghue, M. B.; Liu, H.; Tan, W. *Chem. Commun.* **2010**, *46*, 249−251.
(59) Wu, Y.; Sefah, K.; Liu, H.; Wang, R.; Tan, W. *Proc. Natl. Acad. Sci. U.S.A.* **2010**, *107*, 5−10.
(60) Farokhzad, O. C.; Cheng, J.; Teply, B. A.; Sherifi, I.; Jon, S.; Kantoff, P. W.; Richie, J. P.; Langer, R. *Proc. Natl. Acad. Sci. U.S.A.* **2006**, *103*, 6315−6320.
(61) Gu, F.; Zhang, L.; Teply, B. A.; Mann, N.; Wang, A.; Radovic-Moreno, A. F.; Langer, R.; Farokhzad, O. C. *Proc. Natl. Acad. Sci. U.S.A.* **2008**, *105*, 2586−2591.
(62) Dhar, S.; Gu, F. X.; Langer, R.; Farokhzad, O. C.; Lippard, S. J. *Proc. Natl. Acad. Sci. U.S.A.* **2008**, *105*, 17356−17361.
(63) Sultan, Y.; Walsh, R.; Monreal, C.; DeRosa, M. C. *Biomacromolecules* **2009**, *10*, 1149−1154.
(64) Sultan, Y.; DeRosa, M. C. *Small* **2011**, *7*, 1219−1226.
(65) Feng, L. Y.; Huang, Z. Z.; Ren, J. S.; Qu, X. G. *Nucleic Acids Res.* **2012**, *40*, e122.
(66) Paul, A.; Maji, B.; Misra, S. K.; Jain, A. K.; Muniyappa, K.; Bhattacharya, S. *J. Med. Chem.* **2012**, *55*, 7460−7471.
(67) Derr, N. D.; Goodman, B. S.; Jungmann, R.; Leschziner, A. E.; Shih, W. M.; Reck-Peterson, S. L. *Science* **2012**, *338*, 662−665.
(68) Sharma, R.; Davies, A. G.; Walti, C. *Nanotechnology* **2012**, *23*, 365301.
(69) Wilson, C.; Szostak, J. W. *Chem. Biol.* **1998**, *5*, 609−617.
(70) Oehler, S.; Alex, R.; Barker, A. *Anal. Biochem.* **1999**, *268*, 330−336.
(71) Shcherbakov, D.; Piendl, W. *Electrophoresis* **2007**, *28*, 749−755.
(72) Chen, Z.; Weber, S. G. *TrAC—Trends Anal. Chem* **2008**, *27*, 738−748.
(73) Jing, M.; Bowser, M. T. *Anal. Chim. Acta* **2011**, *686*, 9−18.
(74) Li, J.; Jiang, Z. Y.; Wu, H.; Zhang, L.; Long, L. H.; Jiang, Y. J. *Soft Matter* **2010**, *6*, 542−550.
(75) Tong, W. J.; Song, H. Q.; Gao, C. Y.; Mohwald, H. *J. Phys. Chem. B* **2006**, *110*, 12905−12909.
(76) Tong, W. J.; Dong, W. F.; Gao, C. Y.; Mohwald, H. *J. Phys. Chem. B* **2005**, *109*, 13159−13165.
(77) Pargaonkar, N.; Lvov, Y. M.; Li, N.; Steenekamp, J. H.; De Villiers, M. M. *Pharm. Res.* **2005**, *22*, 826−835.
(78) Jiang, X. M.; Chen, Z. C.; Lv, D. S.; Wu, Q.; Lin, X. F. *Macromol. Chem. Phys.* **2008**, *209*, 175−183.
(79) Angelatos, A. S.; Johnston, A. P.; Wang, Y.; Caruso, F. *Langmuir* **2007**, *28*, 4554−4562.
(80) Kohler, K.; Mohwald, H.; Sukhorukov, G. B. *J. Phys. Chem. B* **2006**, *110*, 24002−24010.